Wave and particle characteristics of earthward electron injections associated with dipolarization fronts

Xiaohua Deng,[1,2] Maha Ashour-Abdalla,[1,3] Meng Zhou,[1,2] Raymond Walker,[1,4] Mostafa El-Alaoui,[1] Vassilis Angelopoulos,[1,4] R. E. Ergun,[5] and David Schriver[1]

Received 17 November 2009; revised 16 May 2010; accepted 27 May 2010; published 28 September 2010.

[1] A comprehensive examination of particle and wave data from multiple Thermal Emission Imaging System (THEMIS) satellites has been made of an electron injection structure in the magnetotail as it propagated earthward from −20 R_E to −11 R_E on 27 February 2009. The electron injection, which was closely associated with a dipolarization front and bursty bulk flows, occurred within a thin plasma boundary layer and had both perpendicular and parallel energization, with very little energy dispersion. The thin plasma boundary layer had a thickness comparable to the ion inertial length and displayed different plasma characteristics at different locations. Strong electromagnetic waves between the lower hybrid frequency and the electron gyrofrequency, as well as electrostatic waves up to the electron plasma frequency, were observed within the thin plasma boundary layers. The two outermost spacecraft at $X = -20.1\ R_E$ and $X = -16.7\ R_E$ detected intense whistler waves, most likely driven by an observed electron temperature anisotropy with $T_\perp/T_\parallel > 1$. Closer to Earth at $X = -11.1\ R_E$, whistlers were not seen, consistent with the observed electron distribution having $T_\perp/T_\parallel < 1$. Near the electron injection region, nonlinear electrostatic structures such as electrostatic solitary waves and double layers were also observed. These nonlinear electrostatic structures can interact with the electron distribution and accelerate electrons; high energy distributions could be generated if the electrons encountered a large number of these structures. The observations show that nonideal MHD, nonlinear, and kinetic behavior is intrinsic to the electron injections with multiscale coupling.

Citation: Deng, X., M. Ashour-Abdalla, M. Zhou, R. Walker, M. El-Alaoui, V. Angelopoulos, R. E. Ergun, and D. Schriver (2010), Wave and particle characteristics of earthward electron injections associated with dipolarization fronts, *J. Geophys. Res.*, *115*, A09225, doi:10.1029/2009JA015107.

1. Introduction

[2] The sharp increases of energetic particle fluxes in the near-Earth tail, known as particle injections, are among the most important and well-known manifestations of magnetospheric Substorm [e.g., *Arnoldy and Chan*, 1969]. The term *injection* has been defined as an increase in the particle flux of finite energy bandwidth [*Kivelson et al.*, 1980]. The energetic particle fluxes in the injections may show either energy dispersion or be dispersionless. Two rather distinct ideas exist concerning the injection processes. The first postulates a time-varying, spatially localized acceleration or heating process with subsequent flow in a quasi-static convection pattern [*McIlwain*, 1974]. The second postulates a time-varying convection pattern which drives earthward flowing plasma with quasi-static properties [*Baker et al.*, 1982; *Li et al.*, 1998]. In either interpretation, the dispersionless flux increases take place in the region where the injection occurs. *Apatenkov et al.* [2007] investigated injections using observations from four Cluster spacecraft on high latitude near Earth tail field lines along with observations at synchronous orbit and argue that bursty bulk flows (BBFs) [*Angelopoulos et al.*, 1992] transport the injections from the tail into the inner magnetosphere. The injection signature in the near-Earth tail also is characterized by a rotation of the magnetic field to a more dipolar configuration [*McPherron*, 1972]. These rapid rotations are frequently called dipolarization fronts (DFs). In a superimposed epoch analysis of dipolarizations observed by the Geotail satellite [*Ohtani et al.*, 2004], the fast flows identified as BBFs were closely associated with the dipolarizations. Recently, *Runov et al.* [2009] used observations from four Thermal Emission Imaging System (THEMIS)

[1]Institute of Geophysics and Planetary Physics, University of California Los Angeles, Los Angeles, California, USA.
[2]Also at Center for Space Science and Technology, Nanchang University, Nanchang, China.
[3]Also at Department of Physics and Astronomy, University of California Los Angeles, Los Angeles, California, USA.
[4]Also at Department of Earth and Space Sciences, University of California Los Angeles, Los Angeles, California, USA.
[5]Department of Astrophysical and Planetary Sciences, University of Colorado, Boulder, Colorado, USA.

0148-0227/10/2009JA015107

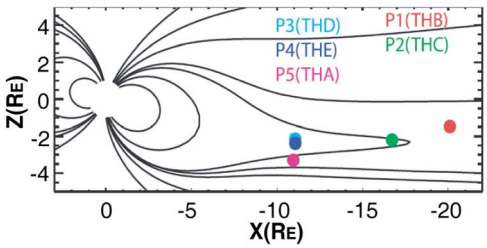

Figure 1. The relative positions of the five Thermal Emission Imaging System (THEMIS) spacecraft in GSM coordinates on 27 February 2009. The THEMIS spacecraft were at midnight and aligned between –20.1 R_E to –11.0 R_E along the Sun-Earth line.

spacecraft, which were lined up in conjunction near midnight during a substorm, to show inward motion from $X \approx -20$ R_E to $X \approx -11$ R_E of the dipolarization fronts and associated particle injection. *Ashour-Abdalla et al.* [2009] investigated the relationship between electron injection and dipolarization fronts during another substorm event observed by multiple THEMIS spacecraft [*Zhou et al.*, 2009]. By coupling global magnetohydrodynamic simulations with large-scale kinetic particle simulations, they demonstrated that betatron and Fermi acceleration were insufficient to account for the observed enhancement of the electron fluxes. They used particle in cell simulations to argue that wave particle interactions may provide the acceleration necessary to account for the injections.

[3] Plasma waves have been observed during substorms on both the Cluster and THEMIS spacecraft [*Le Contel et al.*, 2006, 2009]. In particular, *Le Contel et al.* [2009] reported quasi-parallel whistler emissions before, during, and after local dipolarizations. The observed electron temperature anisotropies ($T_\perp/T_\parallel$) were sufficient to generate the whistler waves. Another type of kinetic behavior in the plasma sheet was reported by *Ergun et al.* [2009], who observed using THEMIS data clear examples of parallel electric fields ($E_\parallel$) in the plasma sheet. They did not carry out a detailed analysis of the role of these structures in the tail but noted that they were associated with BBFs. The structures are very similar to double layers associated with field-aligned currents observed much closer to the Earth in the auroral region [*Ergun et al.*, 2001].

[4] In this paper, we take advantage of the alignment of THEMIS spacecraft, each with its suite of particle and wave instruments, to investigate in detail the electron injection as a function of radial distance, and study its relationship with DFs, BBFs, and plasma waves. In the next section, we discuss the observations from THEMIS P1–P4. In section 3, we summarize the observations and conclude with a discussion of the overall ramifications of this study.

2. Observations

[5] Figure 1 shows the locations of the five THEMIS spacecraft on 27 February 2009. The THEMIS spacecraft were at midnight and aligned between -20.1 R_E to -11.0 R_E along the Sun-Earth line. Figure 2 shows an overview of this event from THEMIS P2 for 15 min before and after the dipolarization events identified by *Runov et al.* [2009]. Data from the fluxgate magnetometer (FGM) [*Auster et al.*, 2008], electrostatic analyzer (ESA) [*McFadden et al.*, 2008] and the solid state telescope (SST) [*Angelopoulos*, 2008] were used in this study and are shown in Figure 2. From top to bottom, we have plotted three components of the magnetic field in geocentric solar magnetospheric (GSM) coordinates, the three GSM components of the flow velocity and ion and electron spectrograms from SST and ESA. Prior to 0753 UT, THEMIS P2 was in the central plasma sheet at $x \approx -16.7$ R_E. Three dipolarizations which are characterized by increases in B_z, can be seen in the magnetic field observations. The sharpest increase in B_Z was at ~0753 UT and was followed by increases at 0757 UT and 0801 UT. Each of the increases in B_z was associated with an increase in the earthward flow velocity (V_x). The increases in velocity are similar to BBFs [*Angelopoulos et al.*, 1992; *Baumjohann et al.*, 1999]. The dipolarization intervals are associated with increases in the energetic ion and electron fluxes (SST and ESA spectrograms). There are decreases in the fluxes of lower energy electrons and ions.

[6] Figure 3 shows a closeup of THEMIS observations of the earthward electron injection associated with dipolarization during the tail conjunction on 27 February 2009. We have plotted 8 min of data around the time of the first dipolarization in Figure 2. In addition to THEMIS P2, we have included data from THEMIS P1 located tailward of P2, and THEMIS P3 located earthward of P2. From top to bottom, we have plotted the magnetic field components in GSM coordinates (Figure 3a), plasma densities (Figure 3b) and temperatures (Figure 3c) for ions (blue) and (Figure 3d) electrons (red), electric fields from particle burst mode waveform data with components parallel (Figure 3e) and perpendicular (Figure 3f) to the ambient magnetic fields, and the energetic electron flux in different energy ranges indicated at the right side in line plot format for ESA observations (Figure 3g) and SST observations (Figure 3h). The electric field observations are from the electric field instrument [*Bonnell et al.*, 2008]. From Figures 3g and 3h, we can see that there is a sudden increase of energetic electron flux observed by P1 (left) near 0751:30 UT, and by P2 (middle) near 0752:30 UT, and then by P3 (right) near 0754:10 UT, respectively. These are marked by the yellow boxes. The SST data are uncalibrated, and therefore the absolute values of moments may have systematic errors, although spot checks of the data show that these systematic errors have no impact on the analysis. The electron injections display very little dispersion. Although the electron energy flux increases by up to an order of magnitude at higher energies >2 keV, there are decreases in the energy flux at energies below 1 keV. All three THEMIS spacecraft observed similar structures. It is evident that there are temporal and local changes in the energetic electrons in addition to the changes caused by the motion of spatial boundaries.

[7] Coincident with the electron injection, very thin plasma boundary layers with rapid changes of plasma density (Figure 3b) and ion temperature (Figure 3c) and electron temperature (Figure 3d) are observed. The electron and ion moments were calculated by combining the data from the ESA and SST instruments. At the electron injection front, the densities (Figure 3b) of ions (blue) and electrons (red)

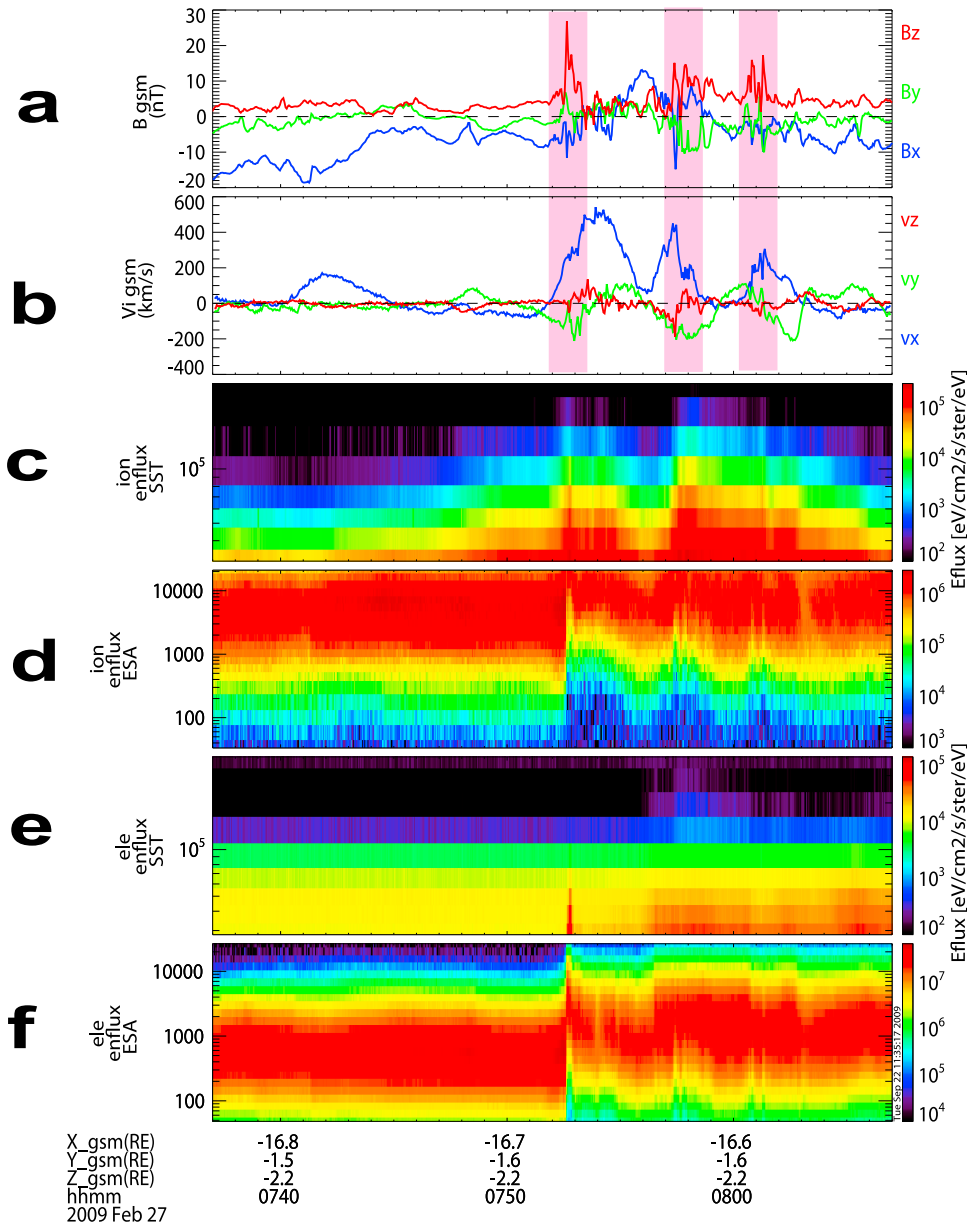

Figure 2. Overview of the observations from THEMIS P2 for 15 minutes before and after the dipolarization events identified by *Runov et al.* [2009]. From top to bottom are the three components of the magnetic field in GSM coordinates, three components of the plasma velocity, and ion and electron energy flux spectrograms from the solid state telescope (SST) and electrostatic analyzer (ESA) instruments. The dipolarizations and increases in the energetic ion and electron fluxes occur during bursty bulk flow events (BBFs).

decrease sharply, whereas the temperatures (Figure 3c) of ions (blue) and (Figure 3d) electrons (red) increase. There are large temperature anisotropies for both ions and electrons. At P1 and P2, the ion temperature (Figure 3c) increases primarily in the direction perpendicular to B creating a temperature anisotropy with $T_\perp > T_\parallel$. There is an electron temperature increase (Figure 3d), in both $T_\perp$ and $T_\parallel$ for all three satellites, however, at P1 $T_\perp \approx T_\parallel$, whereas at P2, $T_\perp > T_\parallel$ and at P3 $T_\perp < T_\parallel$. *Runov et al.* [2009] showed that the earthward propagation speed of the thin plasma layer associated with the dipolarization is ~300 km/s, and its thickness is estimated to be ~400 km [*Runov et al.*, 2009], which is near the ion inertial length of 300 km.

[8] It is important to recall that the electron injection and thin plasma boundary layer are closely related to the magnetic field dipolarization fronts and BBFs (Figure 2). The dipolarizations at P1 and P2 are preceded by small decreases in B_z similar to those reported by *Ohtani et al.* [2004] and *Runov et al.* [2009] and have been shown in full-particle simulations with open boundaries by *Sitnov et al.* [2009].

[9] The electric field instrument (EFI), provided three-axis electric field waveform data with time resolution of 128 Hz in the particle burst mode and 8192 Hz in the wave

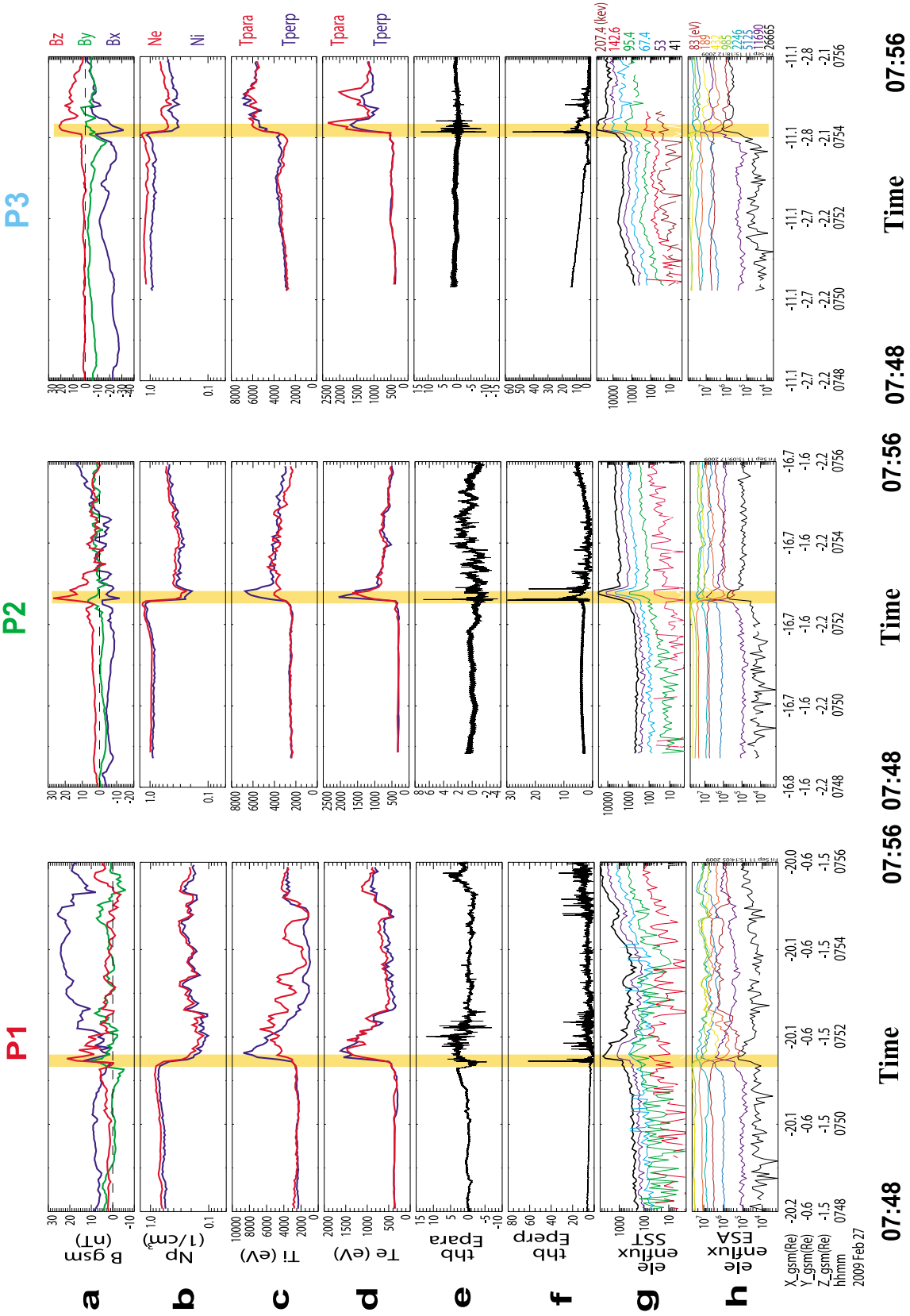

Figure 3. THEMIS observations of earthward electron injection with thin plasma layers associated with depolarization during the tail conjunction on 27 February 2009. From top to bottom are (a) the magnetic fields in GSM, (b) plasma densities for ions (blue) and electrons (red), (c) parallel (red) and perpendicular (blue) temperatures for ions and (d) electrons, (e) parallel and (f) perpendicular electric fields, differential omnidirectional electron flux variations in different energy ranges in line plot form from (g) SST and (h) ESA, for (left)P1, (middle) P2, and (right) P3, respectively.

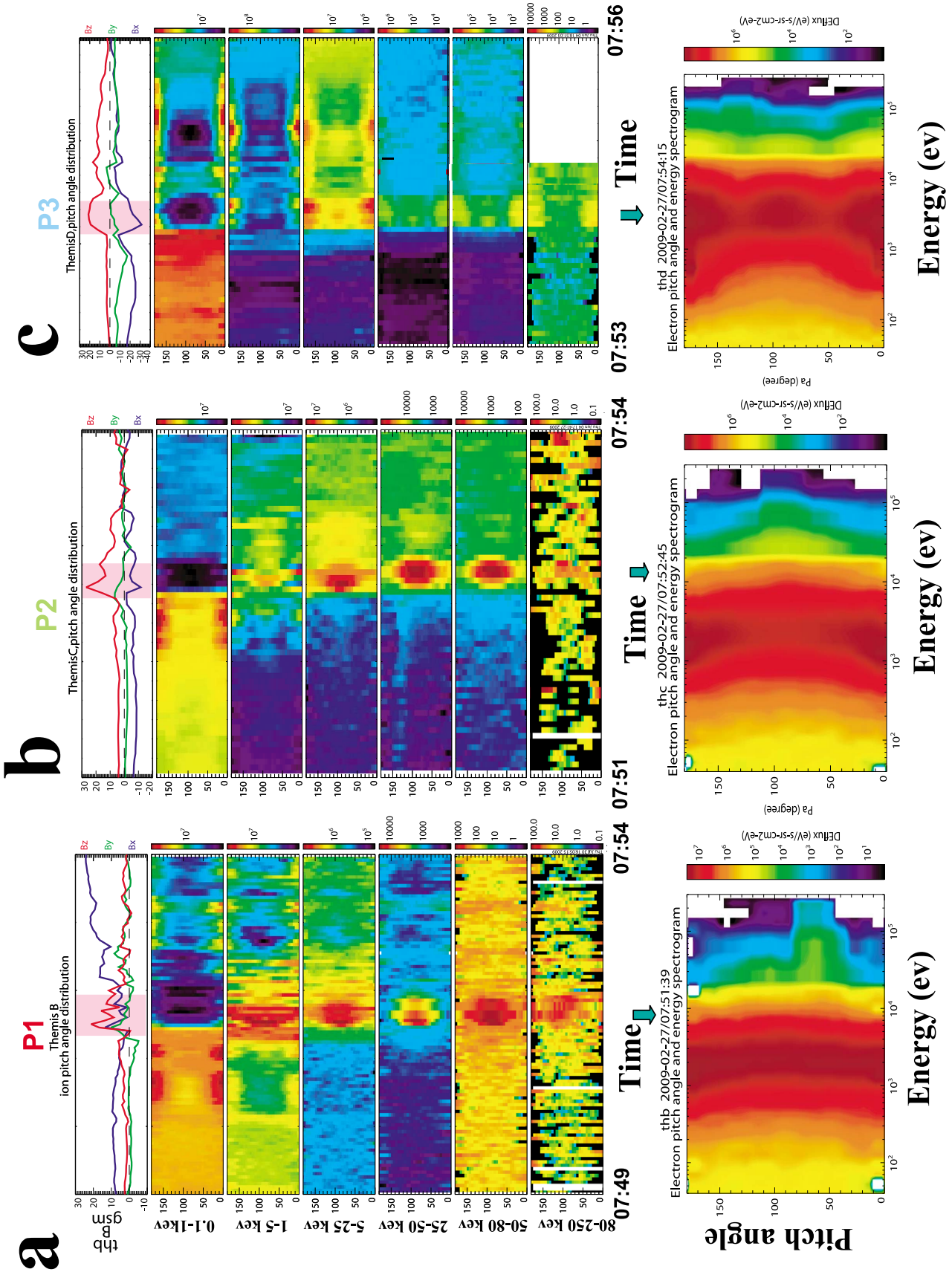
a
b
c
P1
P2
P3
Themis B
ion pitch angle distribution
ThemisC,pitch angle distribution
ThemisD,pitch angle distribution
thb B gsm
0.1-1kev
1-5 kev
5-25 kev
25-50 kev
50-80 kev
80-250 kev
07:49
07:54
07:51
07:54
07:53
07:56
Time
Electron
Pitch angle
Energy (ev)
thb 2009-02-27/07:51:39
Electron pitch angle and energy spectrogram
thc 2009-02-27/07:52:45
Electron pitch angle and energy spectrogram
thd 2009-02-27/07:54:15
Electron pitch angle and energy spectrogram
Pa (degree)
DEflux (eV/s-sr-cm2-eV)

Figure 4

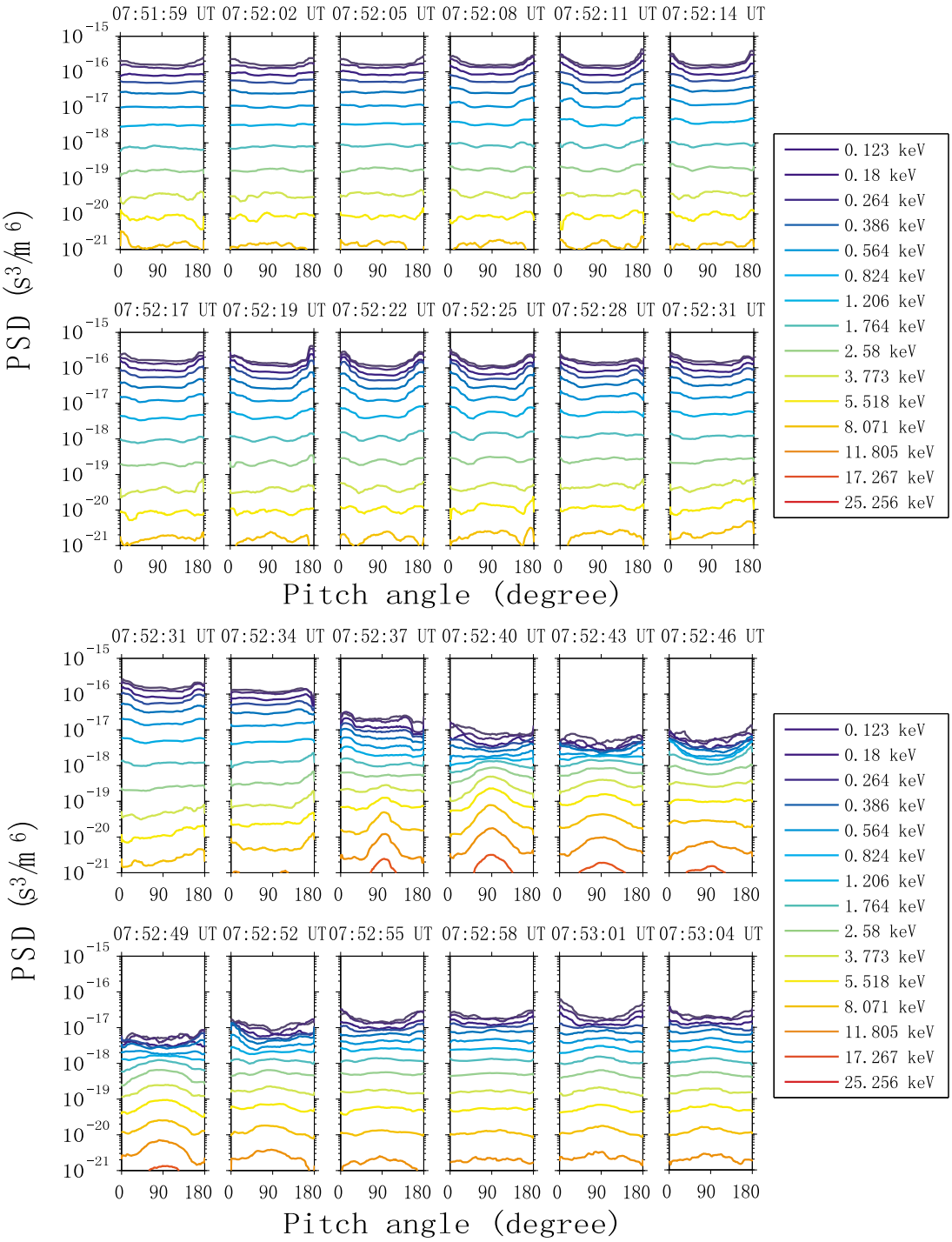

Figure 5. The detailed pitch angle distributions are shown from THEMIS P2 during the electron injection for 15 different energy channels from 0.123 keV to 25.256 keV with an accumulation time of 3 sec. When injection starts at about 0752:34 UT, the increase at higher energies is dramatic and the increase peaks at 90° pitch angle.

Figure 4. The color-coded electron energy flux pitch angle distributions versus time for different energy ranges observed by the THEMIS SST and ESA instruments for (left) P1, (middle) P2, and (right) P3, respectively. The scale on the *y*-axis gives electron pitch angles with 0° (parallel) at the bottom and 180° (anti-parallel) at the top of each image. The top contains the three components of the magnetic field. The next six images contain energy fluxes for 0.1–1 keV, 1–5 keV, 5—25 keV, 25—50 keV, 50—80 keV, and 80—250 keV respectively. On the bottom, the plot shows the differential energy flux in pitch angle versus energy format for P1, P2, and P3, respectively. The times for each plot on the bottom are indicated by the green arrows.

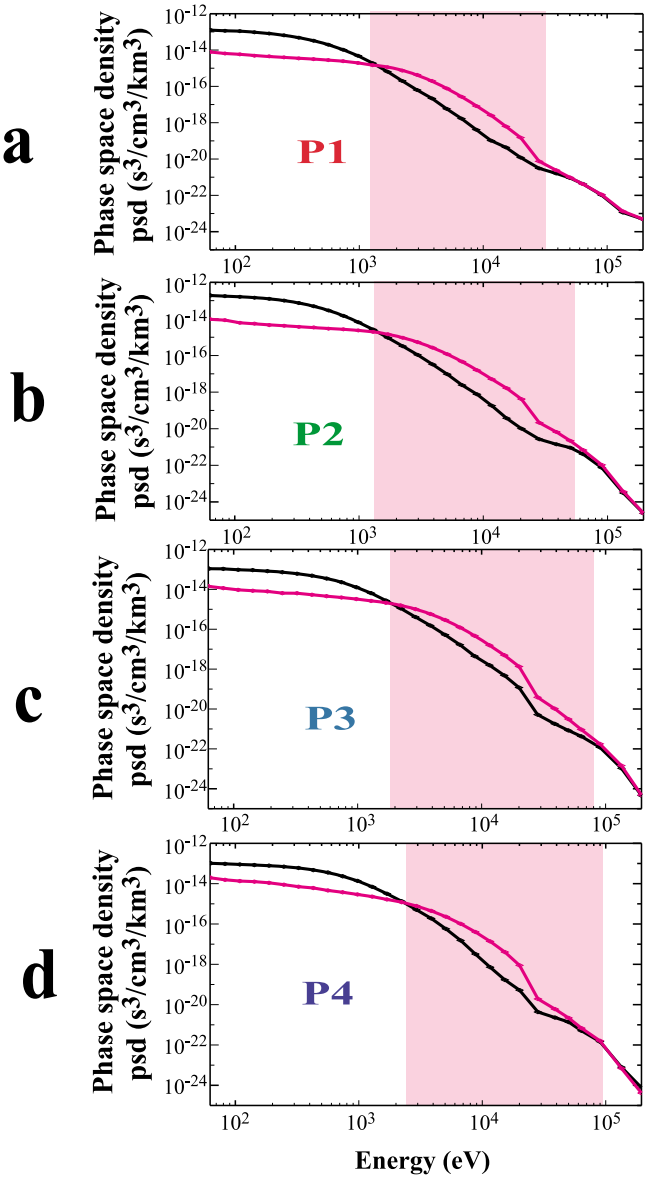

Figure 6. The electron phase space density versus energy obtained before (black) and during (red) electron injection for (a) P1, (b) P2, (c) P3, and (d) P4, respectively. The region between the energies at which the black and red curves cross have been shaded pink.

burst mode [*Bonnell et al.*, 2008]. Figures 3e and 3f show the calibrated 3-D particle burst electric field waveform data along the magnetic field. It is important to note that there is strong enhancement of the electric fields coincident with the sharp flux increases in the energetic electrons at all of the satellites. The electric fields spike up to 10 mV/m in the direction parallel to the magnetic field (Figure 3e) and up to 60 mV/m in the direction perpendicular (Figure 3f) to the ambient magnetic field.

[10] Figure 4 shows color-coded electron energy flux pitch angle distributions versus time for different energy ranges observed by the THEMIS SST and ESA instruments for P1 (left), P2 (middle), and P3 (right), respectively. The scale on the *y*-axis gives electron pitch angles with 0° (parallel) at the bottom and 180° (anti-parallel) at the top of each image. Variations in the magnetic field are shown for reference at the top. We can see that both perpendicular (near 90°) and parallel (0° or 180°) acceleration is observed [*Apatenkov et al.*, 2007]. There are two interesting aspects of the electron pitch-angle behavior: the pancake anisotropy (90° peak) is mainly observed by P1 and P2, whereas the field-aligned anisotropy is mainly observed by P3 and P4 (not shown) during the dipolarization. On the bottom, we have plotted the differential energy flux in a pitch angle versus energy format. The plots are limited to times during which the spacecraft were in the electron injection region at the top. At energies above 20 keV, P1 and P2 mainly observed perpendicular acceleration (near 90°), whereas P3 (and P4) mainly observed parallel acceleration (small angles). An enhancement at pitch angles close to 90° as seen at P1 and P2 is consistent with betatron acceleration. Enhancements at smaller pitch angles as seen at P3 (and P4 not shown) is consistent with Fermi acceleration, which occurs when a particle bounces between mirror points within a flux tube that becomes shorter as it dipolarizes and moves toward the Earth.

[11] We have plotted detailed pitch angle distributions at different times for the electron injection observed by THEMIS P2 in Figure 5. The energies plotted are given on the left. Just prior to the injection (top two rows) the lower energy particles have a butterfly distribution with peaks at small pitch angles. Higher energies are nearly isotropic. Once the injection starts, it proceeds quickly with higher energies (>5 keV) peaking at ~90°, whereas lower energies (<0.5 keV) tend to have a minimum ~90°. For instance, in the third image from the top, the injection starts at about 0752:34 and is clearly evident by 0752:37 (third image). As noted earlier, the phase space density of the lower energy particles decrease by over an order of magnitude, and the phase space density of the higher energies increase dramatically. The increase peaks at 90° pitch angle. In the last row starting at 0752:49, the particle phase space density has started to decrease at high energies and increase at lower energies. It is interesting to note that as the dipolarization front passes over P2, the electron distribution appears to be split into two components within the injection region. The lower energy population (<0.5 keV) is more field-aligned, whereas the higher energy population shows signatures of transverse acceleration.

[12] In Figure 6, we display the electron phase space density versus energy obtained before the dipolarization (black) and during electron injection (pink) for P1 (Figure 6a), P2 (Figure 6b), P3 (Figure 6c), and P4 (Figure 6d), respectively. This format clearly shows the energy dependence of the injections. Note that the phase space densities did not increase for all energies. In fact, at lower energies, the phase space density decreases, whereas at higher energy, the phase space density increases. The flux of electrons in the lower energy range (<1 keV) decreases while the flux increases at energies from 1 keV up to >100 keV. It is interesting to note that the crossing points of the red lines and blue lines move to higher energy from P1 (located at −20.1 R_E) to P2 (−16.7 R_E) and then P4 (−11 R_E). That is, the injection starts at higher energies closer to the near-Earth than in the distant tail. The injection also extends to higher energies in the inner tail (P4).

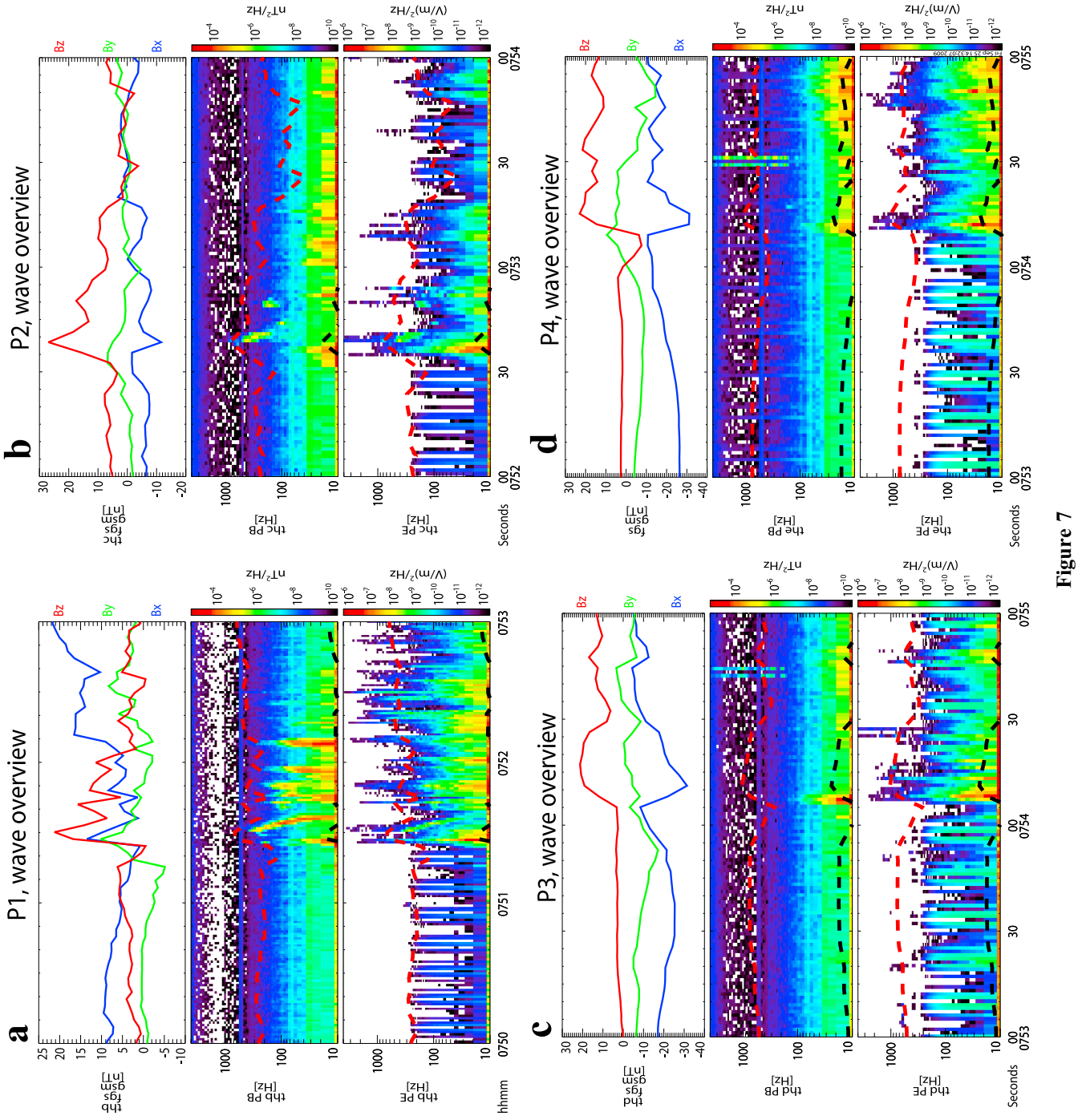
a
P1, wave overview
b
P2, wave overview
c
P3, wave overview
d
P4, wave overview
Bz
By
Bx
thb fgs gsm [nT]
thb PB [Hz]
thb PE [Hz]
thc fgs gsm [nT]
thc PB [Hz]
thc PE [Hz]
thd fgs gsm [nT]
thd PB [Hz]
thd PE [Hz]
fgs gsm [nT]
the PB [Hz]
the PE [Hz]
nT²/Hz
(V/m)²/Hz
hhmm
Seconds

Figure 7

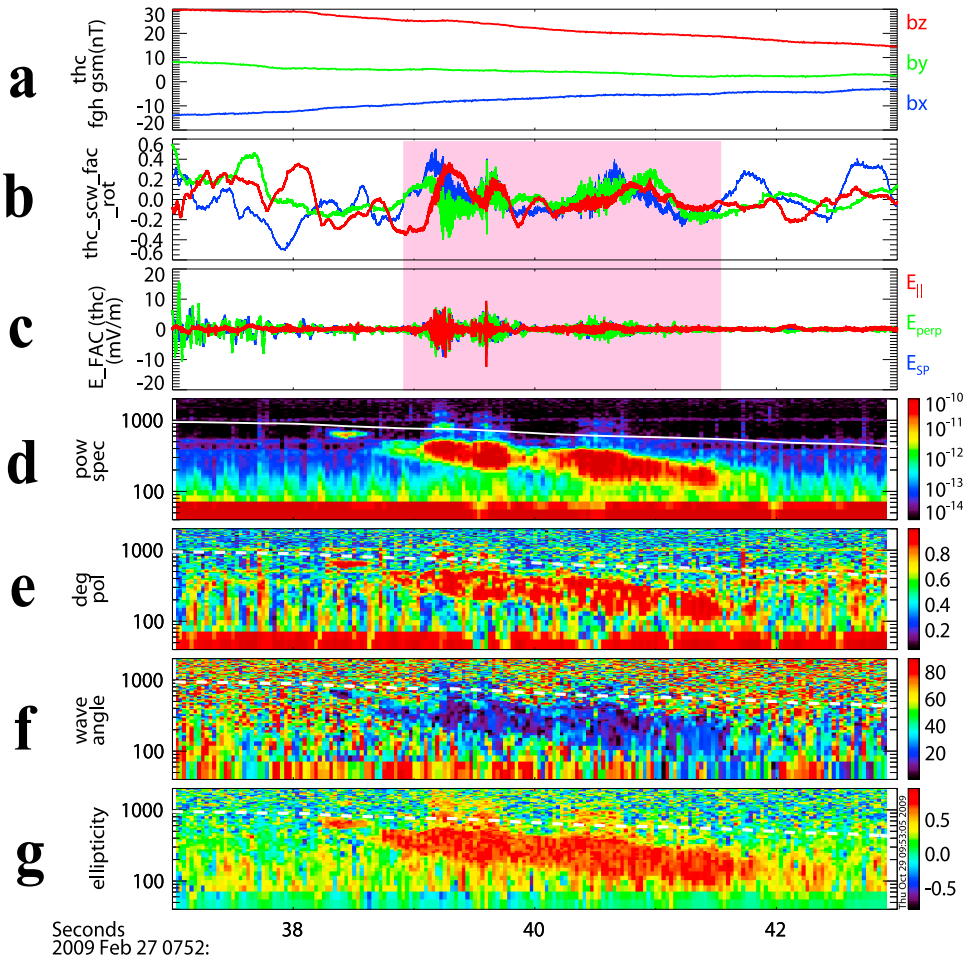

Figure 8. The results of the wave analysis of the wave burst mode data taken of 8192 samples/s on P2. From top to bottom are three components of (a) the magnetic field in GSM coordinates, (b) the perturbation magnetic field in a field-aligned coordinate system, (c) the perturbation electric field in a field-aligned coordinated system, (d) dynamic power spectral density from fluctuations of the B_x component, (e) the degree of polarization, (f) the wave angle, and (g) the ellipticity, respectively. The superimposed white dashed curve corresponds to electron cyclotron frequency.

[13] We now consider the plasma wave activity that occurred at the different satellites during this event. In Figure 7, we have plotted 2 min of data from all four spacecraft, where for reference the three GSM components of the magnetic field are plotted at the top. In the bottom two images, we have plotted frequency time spectrograms of the magnetic field wave (middle) and electric field wave (bottom) power spectral densities. In each spectrogram, we have superimposed dashed traces showing the electron cyclotron frequency (red) and the lower hybrid frequency (black). At all four spacecraft, there is low-frequency power in both the magnetic and electric field spectrograms that start at the time of the dipolarization. In addition, at P1 and P2, there is higher-frequency power primarily in the magnetic field. This power is most evident near the peak in the dipolarization signal.

[14] Using the method of *Samson and Olson* [1980], we have analyzed the polarization characteristics of magnetic fluctuations near the electron injection region with the particle and wave burst mode data from the search coil magnetometers (SCM) [*Le Contel et al.*, 2008]. In particular, during the dipolarization at P2, wave burst mode data collected at 8192 samples/s were available. In Figure 8, we have plotted the results of the wave analysis of the burst mode data. Starting from the top, the first image shows the three components of the magnetic field in GSM coordinates,

Figure 7. Two minutes of wave data from all four spacecraft: (a) P1, (b) P2, (c) P3, and (d) P4. Each plot in Figures 7a–7d show (top) three GSM components of the magnetic field, (middle) frequency time spectrograms of the magnetic field wave, and (bottom) electric field wave power spectral density, respectively. The superimposed dashed traces are at the electron cyclotron frequency (red) and the lower hybrid frequency (black).

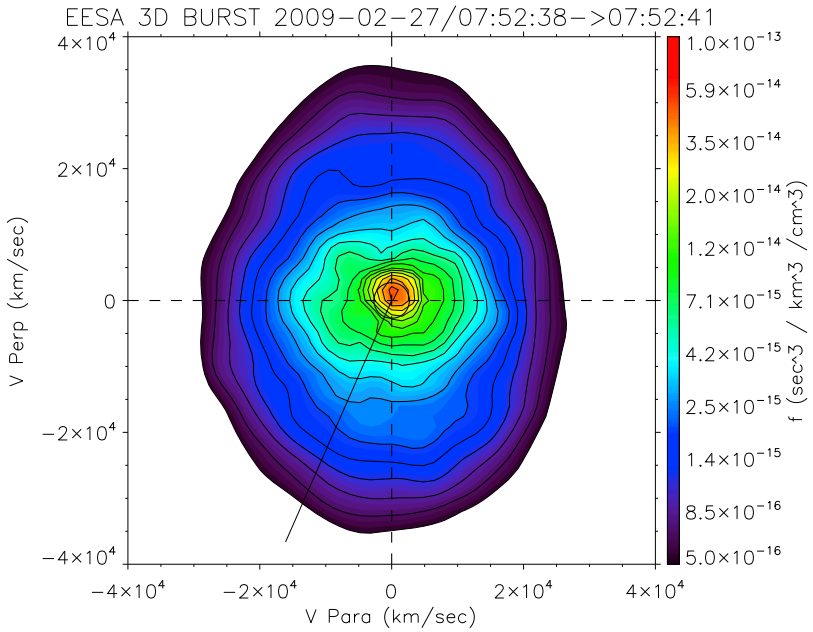

Figure 9. The electron distribution function during the wave burst mode interval shown in Figure 8.

the second and third images show the magnetic and electric fields in a field-aligned coordinate system, respectively, the fourth image shows the dynamic power spectral density from fluctuations of the B_x component, the fifth image shows the degree of polarization, the sixth image shows wave angle, and the bottom shows ellipticity. The wave angle is the angle between the wave vector and the background magnetic field, and the ellipticity is the ratio between the major and the minor axes of the polarization ellipse. The superimposed white dashed curve corresponds to the electron cyclotron frequency. From this high-resolution wave burst data, clear signatures of whistler waves have been identified at frequencies between 200 Hz and 400 Hz. They are right-hand circularly polarized (red in the third image) with ellipticity near 1 (red in the bottom) and propagate parallel or antiparallel to the ambient magnetic field with wave angle near zero (blue region in the fourth image). The broadband whistler emissions have little frequency dispersion, suggesting that the sources are very close to the probe. At this time, the electron perpendicular temperature is larger than the parallel temperature as shown in Figure 3 (middle column, row d). This can be clearly seen in Figure 9, where we have plotted the electron distribution function during the burst interval. The distribution function contours are elongated along the perpendicular velocity axis at higher velocities, which is consistent with an anisotropy-driven whistler mode instability [*Kennel and Petschek*, 1966; *Gary and Karimabadi*, 2006]. Note that the velocity distribution function in Figure 9 shows the two-population characteristic discussed previously in Figure 6, in which the lower energies tend to be field-aligned and the higher energies are transversely aligned.

[15] We have plotted 3-D burst mode electric field data from P2 and P3 in Figure 10. Note that the plotted time intervals are different for each image. The top two images show P2 observations, and the bottom two images show P3 observations. Near the electron injection region, large amplitude nonlinear electrostatic structures, such as electrostatic solitary waves (ESWs) and double layers (DLs) were observed. The ESWs (shaded pink) are characterized by solitary bipolar pulses in the electric field parallel to the background magnetic field [*Matsumoto et al.*, 2003]. Nearer the Earth at P3, double layers (orange) were observed in addition to the ESWs. The DLs have unipolar signatures in the electric field parallel to the background magnetic field [*Temerin et al.*, 1982]. The ESWs and DLs are 3-D structures with signatures in the directions parallel and perpendicular to the ambient magnetic fields. The amplitudes in the parallel component of the ESWs are ~20 mV/m, and the amplitude of the perpendicular components range from 2 mV/m to 6 mV/m. The amplitudes of the parallel component of DLs observed at P3 are ~10 mV/m, whereas the amplitudes of the perpendicular components are <2 mV/m.

3. Summary and Discussion

[16] A study of a dipolarization front that brings together comprehensive particle and wave data from multiple THEMIS satellites has been carried out. Although various aspects related to dipolarization fronts and substorm activity have been examined previously, including particle energization, the thickness and speed of the dipolarization fronts, whistler wave activity, double layers, and electrostatic solitary waves, these have been considered for the most part separately. This study here brings all of these particle and wave measurements together for a particular event as a dipolarization front moves earthward from THEMIS satellite to THEMIS satellite in an effort to understand how they are related and how particle acceleration occurs.

[17] Before discussing the implications of this study, we first summarize the main findings:

[18] 1. The earthward moving dipolarization front on 27 February 2009 was associated with an electron flux increase

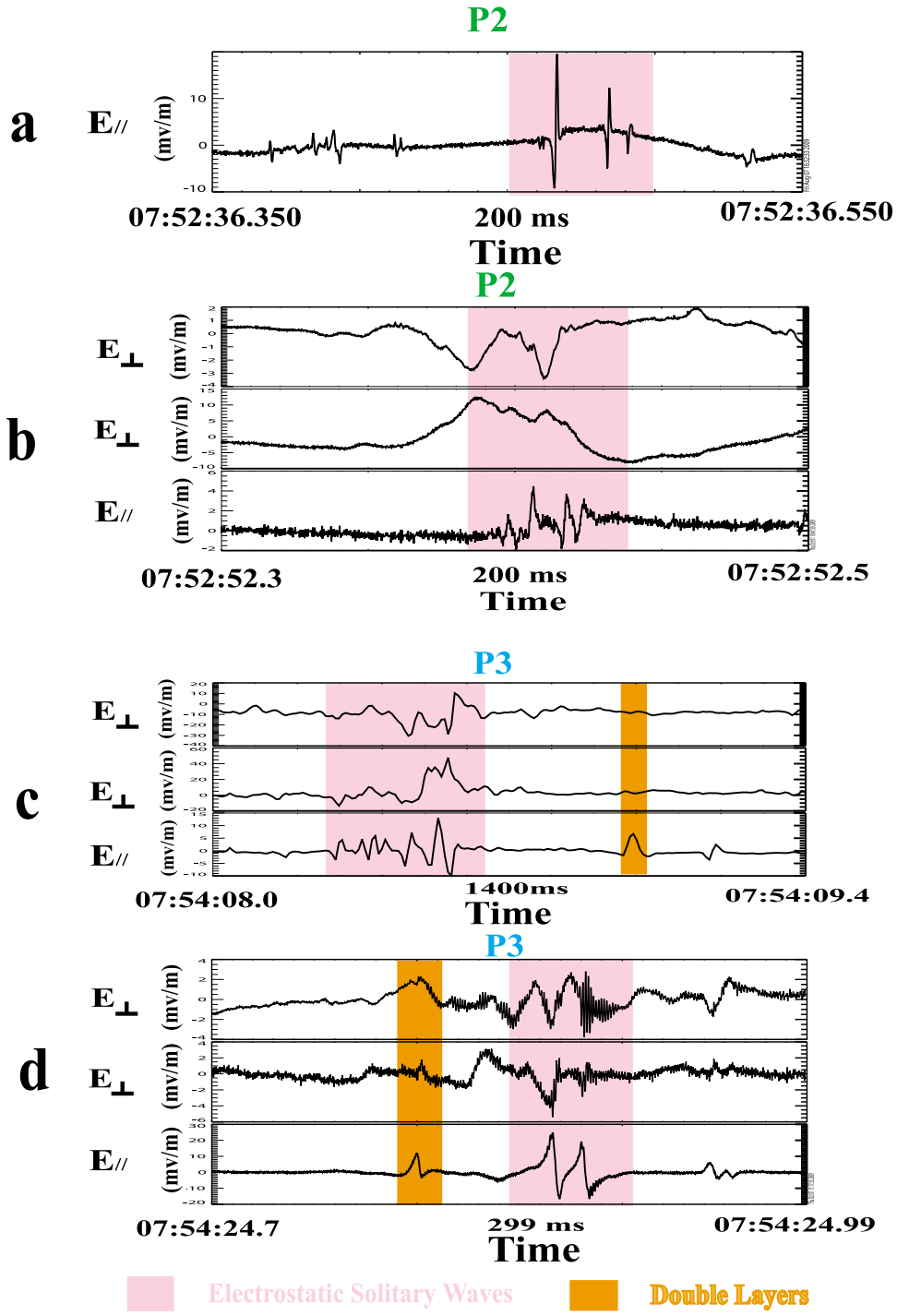

Figure 10. Nonlinear electrostatic structures observed near the electron injection region for P2 and P3. Note that the time intervals plotted are different for each image. (a) $E_{\parallel}$ at P2; (b) all three components of **E** at P2. (c and d) All three components of **E** have been plotted from P3. Electrostatic solitary waves are shaded pink, and double layers are shaded orange.

at energies >2 keV and decrease in the electron energy flux for the lower electron energy population.

[19] 2. In conjunction with the observed changes in the electron energy flux at dipolarization, an enhancement in the wave activity level occurred. In the outer magnetosphere (THEMIS P1 and P2), whistler waves were observed. Closer to the Earth (THEMIS P3 and P4), electrostatic solitary waves and double-layer structures were found.

[20] 3. In the outer magnetospheric region, the perpendicular temperature was greater than the parallel temperature, i.e., $T_{\perp} > T_{\parallel}$, whereas closer to Earth, the temperature anisotropy was reversed such that $T_{\perp} < T_{\parallel}$.

Table 1. Summary of the Wave Observations Made by THEMIS Spacecraft

Event		P_1	P_2	P_3	P_4	P_5
Deng et al. (present study)	Position (RE)	(−20.1, −0.6, −1.5)	(−16.7, −1.6, −2.2)	(−11.1, −2.7, −2.2)	(−11.1, −1.8, −2.4)	
	Wave around the DF	Whistler	Whistler ESW	Double layer & ESW Eperp/Epara=0.25~1	Double layer & ESW	
	Distance to neutral sheet (RE)	0.6	−0.1	−0.2	−0.4	
Le Contel et al. [2009]	Position	(−29, 2.3, −9.)	(−18, 1.6, −5.6)	(−9.5, 1.6, −3.)	(−8.2, 2.5, −2.3)	
	Wave around the DF	No	No	Whistler	Whistler	
	Distance to neutral sheet (RE)	−5.6	−2.2	0.1	0.6	
Ergun et al. [2009]	Position		(−18.4, −2.1, −5.9)	(−9.2, 2.6, −0.9)		(−8.7, 3.6, −1.6)
	Wave around the DF		Double layer & ESW Eperp/Epara =2.5	Double layer & ESW Eperp/Epara = 0.3~1		Double layer & ESW Eperp/Epara =0.7
	Distance to neutral sheet (RE)		−2.7	−1		−0.4

[21] 4. As the dipolarization front passes P2, the electron distribution function appears to be split into two components within the injection region. The lower energy population (<0.5 keV) is more field-aligned, whereas the higher energy population shows signatures of transverse acceleration.

[22] Understanding electron injections as examined here is important because the acceleration of particles and the transport of plasma through the magnetosphere, and specifically the magnetotail, govern magnetospheric structure as well as its dynamics. *Angelopoulos et al.* [1992] and *Nakamura et al.* [2002] reported dipolarization and electron acceleration associated with BBFs. Most previous studies of particle injections have been made at locations near geosynchronous orbit. In this paper, multipoint observations from the five THEMIS probes aligned in conjunction between −20 R_E and −11 R_E in the tail have provided the first observations of earthward dispersionless electron injections with thin plasma boundaries. All four spacecraft were very near the neutral sheet when they observed the electron injection. The dipolarization front, a thin plasma boundary and electron injection region, was observed by each of the satellites and was associated with earthward BBFs (Figure 2). The electron injection front and thin plasma boundary layer propagate earthward at speeds of 300 km/s, and the thickness of the thin plasma boundary is estimated to be 400 km, which is comparable to the ion inertial length [*Runov et al.*, 2009]. In the electron injection region, a very localized and sharp increase of parallel and perpendicular electric fields has been observed. The sharp magnetic field changes could be associated with strong induced electric fields and field-aligned currents [*Aggson et al.*, 1983; *Lui*, 1996]. At THEMIS P1 and P2, the acceleration was primarily at 90° pitch angle, whereas at THEMIS P3 and P4 nearer the Earth, it was primarily field-aligned (Figure 4). The perpendicular acceleration is most likely the result of gyrobetatron and drift betatron acceleration acting respectively on the gyromotion and the drift motion of the particle, whereas the acceleration of particles along the field direction is consistent with Fermi acceleration in which a particle bounces between mirror points within a flux tube that becomes shorter as it dipolarizes and moves toward the Earth. However, during the substorm on 15 February 2008 (see *Zhou et al.* [2009] for a discussion of the observations), *Ashour-Abdalla et al.* [2009] used simulations to argue that betatron and Fermi acceleration were insufficient to account for the electron acceleration and that acceleration by plasma waves or other processes was required. *Smets et al.* [1999] and *Apatenkov et al.* [2007] showed that contracting magnetic flux tube during magnetospheric reconfiguration can provide betatron and Fermi acceleration in a good comparison with observations.

[23] The role of waves and nonlinear electrostatic structures in the dynamics of the Earth's magnetosphere has long been an important topic [e.g., *Deng and Matsumoto*, 2001]. Near the electron injection region, nonlinear 3-D electrostatic structures, including double layers (DLs) and electrostatic solitary waves (ESWs), as well as intense right-hand circularly polarized whistler waves with frequencies up to 400 Hz were observed in the wave burst data. Self-consistent numerical studies have shown that the nonuniformity of the magnetic field plays a key role in the amplification process of whistler mode wave emissions formed at the equator and that nonlinear effects can increase the frequency of the emissions [*Omura et al.*, 2008]. Table 1 summarizes the wave observations at the THEMIS spacecraft during the electron injection. THEMIS P1 and P2 were the most tailward of the spacecraft on 27 February 2009, and both observed whistler waves while the two earthward spacecraft (P3 and P4) did not. The energetic electron distribution functions observed at P1 and P2 were peaked in the perpendicular direction with $T_\perp > T_\parallel$ (see Figures 3, 4, and 9). This is consistent with the local generation of whistler waves. Table 1 also summarizes the whistler mode observations reported during a substorm by *Le Contel et al.* [2009]. They observed whistler mode waves at the two inner most spacecraft and not at the outer spacecraft. However, P1 and P2 were fairly far from the neutral sheet in their study. It is interesting to note that the characteristics of the plasma boundary layers near the Earth (P3 and P4 located near −11 R_e) are quite different from that in the middle tail region (P1 and P2 located at −20 R_e and −16.7 R_e, respectively). At P3 and P4, $T_\perp < T_\parallel$ and thus whistlers were not being locally generated.

[24] The BBF and shear flows can generate Alfvén waves. When Alfvén waves propagate earthward and encounter the thin plasma boundary layers, the large gradients in the plasma and magnetic field can effectively couple large-scale Alfvén waves with kinetic Alfvén waves [*Hasegawa and Chen*, 1975; *Lysak*, 2008; *Johnson et al.*, 2001]. By comparing the Alfvén speed calculated by the local plasma and field parameters and the phase speed estimated by the ratio

(E/B) of the amplitudes of wave fluctuations of electric field (E) over that of the magnetic field (B), we can find that ahead of the electron injection fronts, enhancement of electromagnetic waves with the phase velocity comparable to the Alfvén speed were observed, just at the electron injection fronts with thin plasma boundary layer, greatly enhanced electrostatic like waves with the phase velocities much larger than Alfvén speed were observed. As we know that kinetic Alfvén waves can get a parallel electric field component, break down the "``frozen-in" condition, decouple the plasma from field lines, and play important role in the electron accelerations. The different draft between electrons and ions can also trigger instabilities, and nonline electron structures, such as double layers, electron holes can form. In an inhomogeneous magnetic field, a parallel electric field may form due to the pitch-angle anisotropy mechanism. ESWs were observed at P2, P3, and P4, but not P1 and DLs were found at P3 and P4. The electric field ratio $E_{\perp}/E_{\parallel}$ at P3 is similar to that reported by *Ergun et al.* [2009] near the neutral sheet (shown in Table 1). These observations indicate that strongly nonlinear, kinetic behavior is intrinsic to the electron injection. These nonlinear microscopic effects can contribute to the formation of parallel potential difference along the field lines. Electrostatic DLs have been proposed as an acceleration mechanism in solar flares and other astrophysical objects. Low-altitude satellites have provided direct observation of DLs [*Ergun et al.*, 2001], whose properties and role in electron acceleration have been analyzed using simulations [*Newman et al.*, 2001]. *Ergun et al.* [2009] reported the first direct observations of parallel electric fields carried by DLs in the plasma sheet of Earth's magnetosphere during enhanced magnetic activity. ESWs represent potential or density structures generated out of nonlinear processes. These electron phase-space holes are thought to be important in scattering and energizing electrons by providing dissipation for collisionless reconnection and heating electrons across collisionless shocks [*Drake et al.*, 2003; *Matsumoto et al.*, 2003; *Bale et al.*, 2003]. *Hoshino* and *Shimada* [2002] studied the suprathermal electron acceleration mechanism in a perpendicular magnetosonic shock wave in a high Mach number regime by using a particle-in-cell simulation. They found that shock surfing/surfatron acceleration producing suprathermal electrons occurs in the shock transition region. There is a series of large-amplitude ESWs excited by the Buneman instability, and the electrons are likely to be trapped by ESWs. During the trapping phase, electrons can be effectively accelerated by the shock motional/convectional electric field.

[25] Particle acceleration still remains one of the most challenging aspects of space and astrophysics. The observation of DLs and ESWs reveal that the electrostatic turbulence observed in the electron injection region is coherent and often composed of 3-D small-scale, large-amplitude nonlinear electric field structures. The energy dissipation under these nonlinear electric fields is apparently not provided by conventional turbulent waves. These structures interact with the electron distribution and accelerate electrons by transit time acceleration, and high-energy electrons could be generated when the electrons pass a large number of these structures. The electron injection process is clearly quite complex. Nonideal, strongly nonlinear, kinetic behavior is intrinsic to electron injection with multiscale coupling of MHD, ions, and electrons. We have only begun to investigate the potentially rich multiscale structuring phenomena that result from the coupling of the MHD scale to the scale of electron kinetics. The observations reported here provide clues for the generation and propagation of high energetic electrons and also shed light on the physics and dynamics of magnetotail. Further studies of the coupling in multiscale structured phenomena by combining theory, simulations, and observations should help to elucidate how plasma heating and high-energy particle acceleration are provided in the magnetosphere and in space plasmas in general.

[26] **Acknowledgments.** Research at the University of California Los Angeles was supported by NASA contract NAS5-02099 for the THEMIS mission and NASA grant NNX08AO48G. X. H. Deng was partially supported by the National Natural Science Foundation of China (NSFC) under grants of 40890163, 40640420563 and 307019. We acknowledge the THEMIS investigators for the use of the data and the analysis software. Specifically, we thank C. W. Carlson and J. P. McFadden for the use of ESA data, D. Larson and R. P. Lin for the use of SST data, K. H. Glassmeier, U. Auster, and W. Baumjohann for the use of FGM data, J. W. Bonnell and F. S. Mozer for the use of EFI data, and A. Roux and O. LeContel for the use of SCM data. The computing was carried out on NASA's Columbia Supercomputer. This is UCLA IGPP publication 6464.

[27] Masaki Fujimoto thanks the reviewers for their assistance in evaluating this paper.

References

Aggson, T. L., J. P. Heppner, and N. C. Maynard (1983), Observations of large magnetospheric electric fields during the onset phase of a substorm, *J. Geophys. Res.*, *88*(A5), 3981–3990, doi:10.1029/JA088iA05p03981.

Angelopoulos, V. (2008), The THEMIS mission, *Space Sci. Rev.*, *141*, 5–34.

Angelopoulos, V., W. Baumjohann, C. F. Kennel, F. V. Coroniti, M. G. Kivelson, R. Pellat, R. J. Walker, H. Lühr, and G. Paschmann (1992), Bursty bulk flows in the inner central plasma sheet, *J. Geophys. Res.*, *97*(A4), 4027–4039, doi:10.1029/91JA02701.

Apatenkov, S. V., et al. (2007), Multi-spacecraft observation of plasma dipolarization/injection in the inner magnetosphere, *Ann. Geophys.*, *25*, 801–814.

Arnoldy, R. L., and K. W. Chan (1969), Particle substorms observed at the geostationary orbit, *J. Geophys. Res.*, *74*(21), 5019–5028, doi:10.1029/JA074i021p05019.

Ashour-Abdalla, M., X. Deng, M. Zhou, D. Schriver, and M. El-Alaoui (2009), Particle acceleration via multiscale processes during substorms, Asia Oceania Geosciences Society, Singapore, 11–15 Aug.

Auster, H. U., et al. (2008), The THEMIS fluxgate magnetometer, *Space Sci. Rev.*, *141*(1–4), 235–264, doi:10.1007/s11214-008-9365-9.

Baker, D. N., et al. (1982), Observations and modelling of energetic particles at synchronous orbit on July 29, 1977, *J. Geophys. Res.*, *87*(A8), 5917–5932, doi:10.1029/JA087iA08p05917.

Bale, S. D., F. S. Mozer, and T. S. Horbury (2003), Density-transition scale at quasi-perpendicular collisionless shocks, *Phys. Rev. Lett.*, *91*, 265004.

Baumjohann, W., M. Hesse, S. Kokubun, T. Mukai, T. Nagai, and A. A. Petrukovich (1999), Substorm depolarization and recovery, *J. Geophys. Res.*, *104*(A11), 24,995–25,000, doi:10.1029/1999JA900282.

Bonnell, J. W., et al. (2008), The electric field instrument (EFI) for THEMIS, *Space Sci. Rev.*, *141*(1–4), 303–341, doi:10.1007/s11214-008-9469-2.

Deng, X. H. and H. Matsumoto (2001), Rapid magnetic reconnection in the Earth's magnetosphere mediated by whistler waves, *Nature*, *410*, 557–560.

Drake, J. F., M. Swisdak, C. Cattell, M. A. Shay, B. N. Rogers, and A. Zeiler (2003), Formation of electron holes and particle energization during magnetic reconnection, *Science*, *299*, 873.

Ergun, R. E., Y. J. Su, L. Andersson, C. W. Carlson, J. P. McFadden, F. S. Mozer, D. L. Newman, M. V. Goldman, and R. J. Strangeway (2001), Direct observation of localized parallel electric fields in a space plasma, *Phys. Rev. Lett.*, *87*(4), 045003.

Ergun, R. E. et al. (2009), Observations of double layers in Earth's plasma sheet, *Phys. Rev. Lett.*, *102*,155002, doi:10.1103/PhysRevLett.102.155002.

Gary, S. P., and H. Karimabadi (2006), Linear theory of electron temperature anisotropy instabilities: Whistler, mirror, and Weibel, *J. Geophys. Res.*, *111*, A11224, doi:10.1029/2006JA011764.

Hasegawa, A., and L. Chen (1975), Kinetic process of plasma heating due to Alfvén wave excitation, *Phys. Rev. Lett.*, *35*, 370.

Hoshino, M., and N. Shimada (2002), Nonthermal particle acceleration in shock front region: "Shock surfing accelerations," *Astrophys. J.*, *572*, 880.
Johnson, J. R., C. Z. Cheng, and P. Song (2001), Signatures of mode conversion and kinetic Alfvén waves at the magnetopause, *Geophys. Res. Lett.*, *28*(2), 227–230, doi:10.1029/2000GL012048.
Kennel, C. F., and H. E. Petschek (1966), Limit on stably trapped particle fluxes, *J. Geophys. Res.*, *71*, 1–28, doi:10.1029/JZ071i001p00001.
Kivelson, M. G., S. M. Kaye, and D. J. Southwood (1980), The physics of plasma injection events, p. 385, in *Dynamics of the Magnetosphere*, edited by S.-I. Akasofu, D., D. Reidel, Boston, MA.
Le Contel, O., F. Sahraoui, A. Roux, D. Fontaine, P. Robert, J.-A. Sauvaud, C. Owen, and A. N. Fazakerley (2006), Small scale Cluster observations of current sheet disruptions during substorms, in *Eighth International Conference on Substorms (ICS-8)*, 27–31 March 2006, edited by M. Syrjaeso, and E. Donovan, pp. 143–148, University of Calgary, Calgary, AB, Canada.
Le Contel, O., et al. (2008), First results of THEMIS Search Coil Magnetometers (SCM), *Space Sci.Rev.*, *141*, 509–534, doi:10.1007/s11214-008-9371-y.
Le Contel, O., et al. (2009), Quasi-parallel whistler mode waves observed by THEMIS during near-Earth dipolarizations, *Ann. Geophys.*, *27*, 2259–2275.
Li, X., D. N. Baker, M. Temerin, G. D. Reeves, and R. D. Belian (1998), Simulation of dispersionless injections and drift echoes of energetic electrons associated with substorms, *Geophys. Res. Lett.*, *25*(20), 3763–3766, doi:10.1029/1998GL900001.
Lui, A. T. Y. (1996), Current disruption in the Earth's magnetosphere: Observations and models, *J. Geophys. Res.*, *101*(A6), 13,067– 13,088, doi:10.1029/96JA00079.
Lysak, R. L. (2008), On the dispersion relation for the kinetic Alfvén wave in an inhomogeneous plasma, *Phys. Plasma, 15*, 062901, doi:10.1063/1.2918742.
Matsumoto, H., X. H. Deng, H. Kojima, and R. R. Anderson (2003), Observation of Electrostatic Solitary Waves associated with reconnection on the dayside magnetopause boundary, *Geophys. Res. Lett.*, *30*(6), 1326, doi:10.1029/2002GL016319.
–
-
McFadden, J. P., C. W. Carlson, D. Larson, V. Angelopoulos, M. Ludlam, R. Abiad, B. Elliott, P. Turin, and M. Marckwordt (2008), The THEMIS ESA plasma instrument and in-flight calibration, *Space Sci. Rev.*, *141*, 277–302.
McPherron, R. L. (1972), Substorm related changes in the geomagnetic tail, *Planet Space Sci.*, *20*(9), 1521–1539.
Nakamura, R., et al. (2002), Motion of the depolarization front during a flow burst event observed by Cluster, *Geophys. Res. Lett.*, *29*(20), 1942, doi:10.1029/2002GL015763.
Newman, D. L., M. V. Goldman, R. E. Ergun, and A. Mangeney (2001), Formation of double layers and electron holes in a current-driven space plasma, *Phys. Res. Lett.*, *87*, 255001.
Ohtani, S., M. A. Shay, and T. Mukai (2004), Temporal structure of the fast convective flow in the plasma sheet: Comparison between observations and two-fluid simulations, *J. Geophys. Res.*, *109*, A03210, doi:10.1029/2003JA010002.
Omura, Y., Y. Katoh, and D. Summers (2008), Theory and simulation of the generation of whistler-mode chorus, *J. Geophys. Res.*, *113*, A04223, doi:10.1029/2007JA012622.
Runov, A., V. Angelopoulos, M. I. Sitnov, V. A. Sergeev, J. Bonnell, J. P. McFadden, D. Larson, K.-H. Glassmeier, and U. Auster (2009), THEMIS observations of an earthward-propagating dipolarization front, *Geophys. Res. Lett.*, *36*, L14106, doi:10.1029/2009GL038980.
Samson, J. C., and J. V. Olson (1980), Some comments on the descriptions of the polarization states of waves, *Geophys. J. R. Astr. Soc.*, *61*, 115–129.
Sitnov, M. I., M. Swisdak, and A. V. Divin (2009), Dipolarization fronts as a signature of transient reconnection in the magnetotail, *J. Geophys. Res.*, *114*, A04202, doi:10.1029/2008JA013980.
Smets, R., D. Delcourt, J. A. Sauvaud, and P. Koperski (1999), Electron pitch angle distributions following the dipolarization phase of a substorm: Interball-Tail observations and modeling, *J. Geophys. Res.*, *104*(A7), 14,571–14,576, doi:10.1029/1998JA900162.
Temerin, M., K. Cerny, W. Lotko, and F. S. Mozer (1982), Observations of double layers and solitary waves in the auroral plasma, *Phys. Rev. Lett.*, *48*, 1175–1179.
Zhou, M., M. Ashour-Abdalla, X. H. Deng, M. El-Alaoui, D. Schriver, and Y. Pang (2009), THEMIS observations of multiple dipolarization fronts and associated wave characteristics in the near-Earth magnetotail, *Geophys. Res. Lett.*, *36*, L20107, doi:10.1029/2009GL040663.

M. Ashour-Abdalla, V. Angelopoulos, X. Deng, M. El-Alaoui, D. Schriver, R. Walker, and M. Zhou, Institute of Geophysics and Planetary Physics, University of California Los Angeles, Los Angeles, CA 90095, USA. (dengxhua@gmail.com)
R. E. Ergun, Department of Astrophysical and Planetary Sciences, University of Colorado, Boulder, CO 80309, USA.